

Passive On-Chip Superconducting Circulator Using a Ring of Tunnel Junctions

Clemens Müller,^{1,2,*} Shengwei Guan,¹ Nicolas Vogt,³ Jared H. Cole,³ and Thomas M. Stace¹

¹ARC Centre of Excellence for Engineered Quantum Systems, School of Mathematics and Physics,
The University of Queensland, Brisbane, Queensland 4072, Australia

²Institute for Theoretical Physics, ETH Zürich, 8093 Zürich, Switzerland

³Chemical and Quantum Physics, School of Science, RMIT University, Melbourne, Victoria 3001, Australia



(Received 12 October 2017; published 25 May 2018)

We present the design of a passive, on-chip microwave circulator based on a ring of superconducting tunnel junctions. We investigate two distinct physical realizations, based on Josephson junctions (JJs) or quantum phase slip elements (QPS), with microwave ports coupled either capacitively (JJ) or inductively (QPS) to the ring structure. A constant bias applied to the center of the ring provides an effective symmetry breaking field, and no microwave or rf bias is required. We show that this design offers high isolation, robustness against fabrication imperfections and bias fluctuations, and a bandwidth in excess of 500 MHz for realistic device parameters.

DOI: [10.1103/PhysRevLett.120.213602](https://doi.org/10.1103/PhysRevLett.120.213602)

Microwave circulators [1,2] are ubiquitous microwave circuit elements [3–5] for signal routing and signal or control isolation. They are also key nonreciprocal elements for realizing chiral quantum optics [6] with microwave photons as well as for microwave photon detection [7] and rectification [8,9]. Commercial, passive circulators are wave-interference devices based on the Faraday effect, which require permanent magnets to break time-reversal symmetry. Size, and their strong magnetic fields, make them unsuited to large-scale integration with superconducting circuits, presenting a hurdle for scaling up superconducting quantum technology.

With the exception of Koch *et al.* [10], most recent approaches to this problem use active devices, based on nonlinear mixing phenomena [11–14] or engineered interplay of driving and dissipation [15–17]. These proposals rely on careful engineering of phase relations between several input and drive fields. Using an rf-driven inductive bridge circuit, Kerckhoff *et al.* [18] demonstrated bandwidths ~ 100 MHz and tuneable center frequency [19,20]. Passive unidirectional devices based on quantum Hall edge modes [21,22] have been demonstrated [23,24]. However, there are challenges to fabricating these elements in a superconducting circuit.

In this Letter, we provide a detailed theoretical analysis of a fully passive, integrated superconducting microwave circulator realized as a ring of tunnel junctions. We simultaneously analyze two implementations of the system: one based on Josephson junctions (JJs), which are in common use for quantum information applications [25–27], and the other based on quantum phase slip (QPS) wires [28]. QPS junctions are dual to JJs under the exchange of voltage and current [28], and they have recently been employed to observe coherent quantum phase slips [29] and as the basic building block of a new type of flux qubit [30,31]. The underlying mathematical

description of these circuit elements is a precise duality; however, they have different noise, fabrication, and geometric characteristics, so that the two implementations may be apposite to different applications or materials.

The basic physics behind our circulator proposal is the nonlocal phase accumulation in the Aharonov-Casher effect for QPS devices, or its dual, the Aharonov-Bohm effect for JJ devices. Both effects arise from the nonlocal topological mutual phase that charge and flux quanta acquire as they are transported around one another.

The operation of our proposal is similar to that of Koch *et al.* [10], but with a number of significant theoretical and practical differences. It does not require extraneous resonators in the devices, nor any active microwave or rf circuitry, both of which simplify and substantially shrink the circuit. Further, we calculate scattering matrices in a fully dynamic picture that includes the internal degrees of freedom of the circulator without relying on an approximate perturbative treatment. Going beyond a linearized, harmonic approximation enables us to quantify the performance of the device at high coupling energies and with high fluxes, both of which preclude perturbative treatments. We show that with experimentally reasonable parameters, passive on-chip circulators can be built with bandwidths ~ 500 MHz, and with moderate photon flux.

Hamiltonian.—To facilitate this dual description, we refer to the diagram in the center of Fig. 1. External ports (numbered $j = 1$ to 3) are coupled to “segments” (circles) arranged in a ring, with canonical “momenta” n_j . The segments of the ring are mutually coupled through tunneling elements (squares), characterized by a tunneling energy E_T and a “mass” term m_T . The ring of segments encircle a central bias, X , providing a time-reversal-symmetry-breaking (effective) magnetic field.

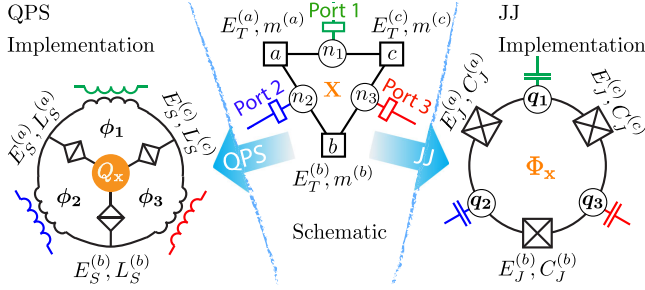


FIG. 1. Center: Schematic representation of the circulator, consisting of three ports connected via coupling elements to the numbered nodes of the ring to the coordinate n_j associated with node j . A central ring bias X is conjugate to n_j . Nodes of the ring are mutually coupled by tunneling elements with tunneling energy $E_T^{(k)}$ and “mass” $m_T^{(k)}$. Notionally, the tunneling elements are identical. Differences lead to imperfect operation. Left: The QPS implementation of the scheme using flux tunneling and capacitive bias. Here $n_j \rightarrow \phi_j/\Phi_0$ are coupled inductively to the external lines, $E_T^{(k)} \rightarrow E_S^{(k)}$ is the phase slip energy, $m_T^{(k)} = L_S^{(k)}$ is the QPS inductance, and $X \rightarrow Q_x/(2e)$ is the linked charge. Right: The JJ implementation of the scheme relying on charge tunneling and inductive bias. Then $n_j \rightarrow q_j/(2e)$ is coupled capacitively to the external lines, $E_T^{(k)} \rightarrow E_J^{(k)}$ is the Josephson energy, $m_T^{(k)} = C_J^{(k)}$ is the JJ capacitance, and $X \rightarrow \Phi_x/\Phi_0$ is the linked flux.

Physically, in the QPS implementation, the segment degrees of freedom correspond to fluxes threading the spokes of the ring structure, illustrated on the left of Fig. 1; i.e., $n_j \rightarrow \phi_j/\Phi_0$, and the central bias is a charge bias, $X \rightarrow Q_x/(2e)$. The coupling to external degrees of freedom is realized via a coupling inductance L_C with an associated coupling mass term m_C . Additionally, each segment has a parasitic inductance L_G , corresponding to a final mass term m_G in the general description. Conversely, in the JJ implementation, the segment degrees of freedom correspond to charges at the nodes between two Josephson junctions, as illustrated on the right of Fig. 1; i.e., $n_j \rightarrow q_j/(2e)$, and the central bias is a flux bias, $X \rightarrow \Phi_x/\Phi_0$. Coupling to the ring is realized capacitively, $m_C = C_C$, and each node has an additional parasitic capacitance $m_G = C_G$. In both cases, eigenmodes of the ring have flux or charge currents circulating around the ring, which acquire phases dependent on the central bias X , through the Aharonov-Casher or Aharonov-Bohm effect [32,33]. Interference between different ring excitations leads to the nonreciprocity required for circulation.

The quantized Hamiltonian for the ring is [10,34]

$$H_{\text{Ring}} = \frac{p_0^2}{2} (\hat{\mathbf{n}} - \mathbf{N}_S) \mathbb{M}^{-1} (\hat{\mathbf{n}} - \mathbf{N}_S) - E_T \sum_j \cos [2\pi(\hat{x}_{j+1} - \hat{x}_j - X/3)], \quad (1)$$

where $\hat{\mathbf{n}} = \{\hat{n}_1, \hat{n}_2, \hat{n}_3\}$ are dimensionless dynamical variables, $\mathbf{N}_n = \{N_S^{(1)}, N_S^{(2)}, N_S^{(3)}\}$ are the classical bias offsets for each segment, $\mathbb{M} = m_\Sigma \mathbb{1}_3 - m_T$ is the mass tensor, and \hat{x}_j is the conjugate variable to \hat{n}_j ; i.e., $[\hat{n}_j, \hat{x}_j] = i$. $m_\Sigma = 3m_T + m_C + m_G$ represents an effective total mass of excitations in the ring and provides the scale of the kinetic energy term. Here p_0 plays the role of zero-point “momentum” in the Hamiltonian and depends on the physical implementation chosen: for QPS devices, $p_0 = \Phi_0$ is the superconducting flux quantum; for JJ devices, $p_0 = 2e$ is the Cooper pair charge. Equation (1) assumes a rotationally symmetric ring, where all mass and tunneling energies are equal. Generalizing to disordered structures simply changes the mass tensor and the tunneling energies, cf. S.1 and S.5 of the Supplemental Material [35].

We change from local to collective coordinates: $\hat{n}_1' = \hat{n}_1$, $\hat{n}_2' = -\hat{n}_2$, and $\hat{n}_3' = \hat{n}_1 + \hat{n}_2 + \hat{n}_3 = N_0$. The latter is the conserved total charge of the ring (since $\partial H/\partial \hat{x}_3' = 0$), so that the Hamiltonian becomes

$$H_{\text{Ring}} = \frac{p_0^2}{m_\Sigma} ((\hat{n}_1' - (N_0 + N_S^{(1)} - N_S^{(2)})/2)^2 + (\hat{n}_2' + (N_0 + N_S^{(2)} - N_S^{(3)})/2)^2 - \hat{n}_1' \hat{n}_2') - E_T (\cos(2\pi(x_1' - X/3)) + \cos(2\pi(x_2' - X/3)) + \cos(2\pi(x_1' + x_2' + X/3))). \quad (2)$$

The value of N_0 is fixed to its ground-state value by the choice of segment bias parameters \mathbf{N}_S [10].

The ring couples to external waveguides at each port, described by the Hamiltonian $H_{\text{WG}} = \sum_{k,j} \omega_k \hat{a}_{k,j}^\dagger \hat{a}_{k,j}$, where k labels waveguide modes and j labels the port number. Details on the derivation of H_{Ring} and the waveguide coupling are given in S.1 of the Supplemental Material [35].

Scattering calculations.—For the purposes of this Letter, we assume coherent field inputs at each port, and we quantify the scattering of waveguide modes from the ring structure using the SLH formalism [8,36], which allows us to calculate output field amplitudes and photon fluxes. We note that the SLH formalism can be adapted to nonclassical input fields [37–39]. Assuming single mode input, the time evolution of the density matrix for the open ring, ρ , satisfies the master equation

$$\dot{\rho} = -i[H_{\text{SLH}}, \rho] + \sum_j \mathcal{D}[b_j]\rho, \quad (3)$$

with $H_{\text{SLH}} = H_{\text{Ring}} + H_{\text{D}}$ and

$$H_{\text{D}} = -\frac{i}{2} \sum_j g_k (\alpha_j e^{-i\omega_k t} q_+^{(j)} + \text{H.c.}), \quad (4)$$

$$b_j = g_k q_-^{(j)} + \alpha_j e^{-i\omega_k t} \mathbb{1}, \quad (5)$$

where α_j is the field amplitude of the incoming signal in transmission line j at frequency ω_k . The frequency-dependent coupling strengths g_k are calculated in S.1 of the Supplemental Material [35] and depend on the physical realization. The outgoing field amplitudes β and photon fluxes B into port j are then given by

$$\beta_j = \text{Tr}\{b_j\rho\}, \quad B_j = \text{Tr}\{b_j^\dagger b_j\rho\}. \quad (6)$$

To calculate scattering dynamics, we first diagonalize H_{Ring} in a truncated Hilbert space of the dynamical variables, $\hat{n}'_{1,2}$. Retaining eigenmodes with eigen-numbers $n'_{1,2} = -4, -3, \dots, 4$ is sufficient to accurately describe low-energy ring modes, $\{|E_0\rangle, |E_1\rangle, |E_2\rangle, \dots\}$. We then further truncate the ring Hilbert space to the lowest l modes for scattering calculations. Typically, $l = 3$ to 5 is sufficient for calculating scattering matrices, due to the strongly anharmonic spectrum of the ring. Apart from controlled truncations, we do not make secular or other approximations in H_{Ring} .

We characterize circulation using the steady-state photon-flux scattering matrix \mathbb{S} , which relates the input and output photon fluxes in each port, $\mathbf{B} = \mathbb{S}\mathbf{A}$, with the vector of input photon fluxes $\mathbf{A} = \{|\alpha_1|^2, |\alpha_2|^2, |\alpha_3|^2\}$. The scattering matrix elements are given by $S_{ij} = \lim_{t \rightarrow \infty} B_i(t)/|\alpha_j|^2 \geq 0$. For an ideal, passive, three-port clockwise circulator, we expect

$$\mathbb{S} = \begin{pmatrix} 0 & 1 & 0 \\ 0 & 0 & 1 \\ 1 & 0 & 0 \end{pmatrix}. \quad (7)$$

The scattering of photons from the ring is mediated by excitations of the ring modes. Notionally, the central bias is tuned so that the relevant ring modes are antidegenerate with respect to the signal frequency ω_k ; i.e., for any ring mode with eigenenergy $\omega_k + E_r$, there is a dual mode with eigenenergy $\omega_k - E_r$. At this tuning point, the scattering matrix becomes maximally nonreciprocal, leading to perfect circulation. Here, we choose the bias point so that circulation proceeds clockwise. We note that there is another bias point where the circulation is reversed; see S.3 of the Supplemental Material [35].

Here, we choose circuit parameters that are feasible for both QPS and JJ implementations, as detailed in S.3 of the Supplemental Material [35]. The tunneling energy is $E_T/\hbar = 15$ GHz, and the kinetic energy term $E_\Sigma/\hbar = 7.80$ GHz. The segments are biased equally with $N_S^{(k)} = N_{S,\text{opt}} = 1/3$, such that the conserved charge of the ground state is $N_0 = 1$. For this choice, we find perfect clockwise circulation at a central bias of $X_{\text{opt}} = 0.356$ and with an input signal frequency of $\omega_{\text{opt}} = 12.293$ GHz. At this optimal point, the coupling strength to the waveguides is

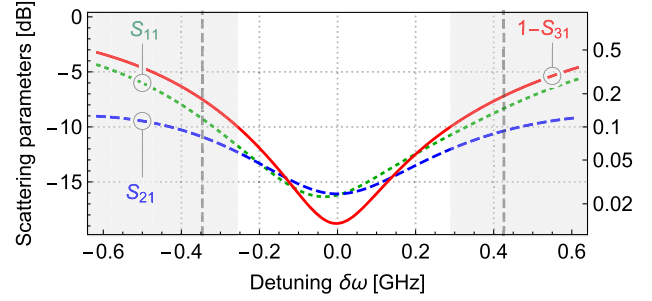


FIG. 2. Scattering parameters in dB as a function of detuning from the optimal signal frequency, $\delta\omega = \omega_k - \omega_{\text{opt}}$. Vertical dashed lines indicate the positions of excited states of the ring, which get transiently excited in the scattering process (see S.4 of the Supplemental Material [35]). The bandwidth at the -10 dB point is > 500 MHz, as indicated by the grey shaded areas.

$g_{\text{opt}} = 1.832$ GHz. This value is large, but experimentally feasible [40,41]. Since $g_{\text{opt}} \ll \omega_{\text{opt}}$, the rotating wave approximation implicit in the SLH formalism is still reasonable. The circulation characteristics at different input frequencies ω_{in} can be found by simple scaling of all energies in the problem by the desired ratio $\omega_{\text{in}}/\omega_{\text{opt}}$.

Bandwidth and nonlinearity.—Figure 2 shows the spectral response of the ring to a weak coherent field incident on port 1, with ideal operating parameters for clockwise circulation. We achieve an insertion loss approaching -20 dB with reflection and isolation both below -15 dB. The performance of the circulator degrades to -10 dB at detunings of $\sim \pm 250$ MHz, so that the -10 dB bandwidth exceeds 500 MHz.

The ring structure is realized as a coherent, nonlinear superconducting device, so it has an anharmonic spectrum and will saturate at sufficiently high powers. Since we diagonalize H_{Ring} nonperturbatively, the SLH formalism enables us to quantify the nonlinear response of the system [36] to continuous incident fields. Figure 3 shows the normalized output flux of the circulator versus input powers. The 1 dB compression point, where performance degrades by 1 dB relative to the ideal, linear case is at -156 dBm, corresponding to $\sim 10^5$ incident photons per

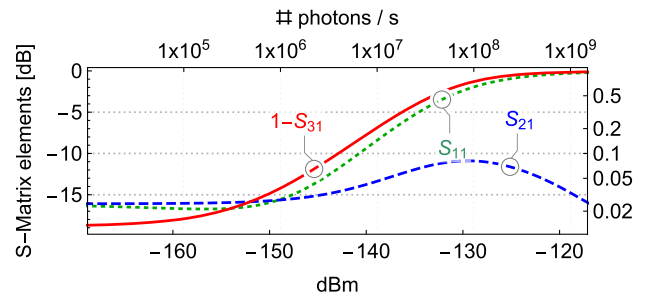


FIG. 3. S -matrix elements (in dB) as a function of input power at the optimal signal frequency and central bias, demonstrating the strong nonlinearity of the ring.

second. Useful circulation extends much further in power, with 10 dB of isolation at -140 dBm.

For transient incident fields, e.g., for a Fock-state with some specific temporal envelope, we expect that dispersion within the transmission window will induce envelope distortion, analogous to Refs. [7,38].

Noise and disorder.—As in other circulator proposals, for ideal operation our scheme requires precise control of parameters. In our design this is the central bias, X , and the offset biases of each segment $N_S^{(j)}$, as well as precise fabrication of the nodes, so that the tunneling and mass terms are identical. In reality, all of these are subject to variation—either drifts in the bias parameters due to environmental noise, or fabrication imperfections, which are built into the device.

Analyzing the effect of such imperfections, we focus on the quasistatic noise case, where the dynamical timescales of the noise processes are slower than the scattering. For the high-bandwidth devices we are considering here, and at moderately low input powers, the ring will stay predominantly in its ground state at all times during operation so that we can neglect decoherence due to the nonradiative decay of ring states. For the strong loss case, where nonradiative decay dominates over the coupling to the waveguides, circulation suffers as photons are lost to the environment. Since nonradiative rates of modern superconducting devices are much smaller than the timescale of circulation defined by the bandwidth, we neglect such processes in the following. Additionally, the eigenenergies of all ring states for the parameters chosen are > 5 GHz and thus well above usual operational temperatures of superconducting quantum circuits ~ 10 mK ≈ 200 MHz. We now quantify the effect of quasistatic variations away from ideality for ring parameters.

The central bias controls the degree of nonreciprocity through changes in the eigenstates of the ring. Figure 4 shows the variation of S_{31} as the central bias is tuned away

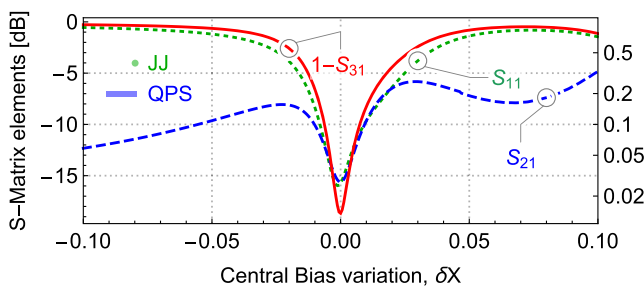


FIG. 4. S -matrix elements as a function of the variation in the central bias parameter, $\delta X = X - X_{\text{opt}}$ (in dB). For the JJ ring, $X = \Phi_X/\Phi_0$; for the QPS ring, $X = Q_X/(2e)$. The notional output is to port 3; outputs to other ports arise from bias variations. The bars in the left of the figure indicate typical variation in the central bias for a JJ-based implementation due to flux noise [42], and a QPS-based implementation due to charge noise [43].

from the optimal point X_{opt} . Evidently, good circulation is maintained as long as fluctuations in the central bias are kept below $\sim 1\%$. Also shown are bars (bottom left) indicating typical fluctuations in the central bias for the two implementations we consider. In this case, flux noise in the JJ implementation is exceedingly small, $\sim 10^{-4}\Phi_0$ [42], whereas charge noise in the QPS implementation is at the $10^{-2}(2e)$ level [43].

Figure 5 shows contours of S_{31} as two of the three segment biases, $N_S^{(1,2)}$, are varied by $\pm 0.1 p_0$. Typical scales for slow variations are shown in the error disks at bottom left. In this case, charge noise in the JJ implementation is at the $10^{-2}(2e)$ level, whereas flux bias noise in the QPS implementation is not visible on this scale. In either case, the system is relatively insensitive at the scale of these variations. We note that variation of the third segment bias, $N_S^{(3)}$, is quantitatively similar to variations in $N_S^{(2)}$.

Lastly, Fig. 6 shows the effect of fabrication imperfections on two of the tunneling energies, $E_T^{(a,b)}$. These are likely to be more variable than the mass terms, since the tunneling is exponentially dependent on device geometry. We note that when calculating scattering with imperfect tunnel junctions, optimal circulation occurs at different bias points for each realization of disorder. Since fabrication disorder is static, this type of variation can be taken into account at initial tuneup of the devices, and each point in Fig. 6 represents an independent optimization of the central bias X and the segment biases $N_S^{(k)}$. Independent variations of the segment biases can partially counteract the asymmetry in junction parameters, evident from the large plateau in Fig. 6. Historically, more effort has been spent optimizing JJ fabrication than QPS devices, so JJ parameters are currently under better experimental control. At the bottom

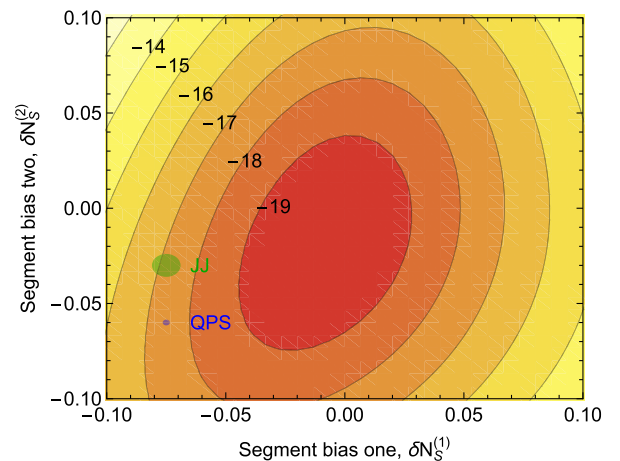


FIG. 5. Effect of deviations in the node bias on the forward transmittance $1 - S_{31}$ (in dB), with $\delta N_S^{(k)} = N_S^{(k)} - N_{S,\text{opt}}$. The disks at the left of the diagram indicate the scale of typical slow bias fluctuations in JJ devices due to charge noise [43] and in QPS devices due to flux noise [42].

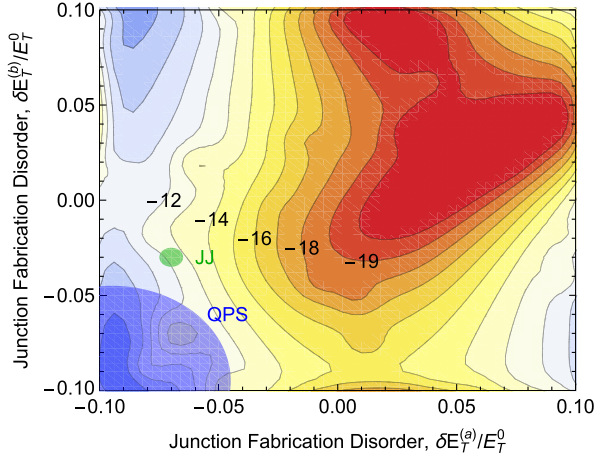


FIG. 6. Effect of imperfections in the tunneling energies $E_T^{(a,b)}$ on forward transmittance $1 - S_{31}$ (in dB). For each point in parameter space, central bias X and segment biases $N_S^{(k)}$ are optimized independently to find maximum forward transmission. The disks at the left indicate the scale of fabrication disorder in JJ [44,45] and QPS devices [30,46].

left, disks indicate a typical scale for the reproducibility of the tunneling energy for JJ, $\sim 1\%$, and QPS, $\sim 10\%$, when comparing junctions fabricated simultaneously on the same chip. We have also simulated the effect of disorder in other Hamiltonian parameters and find qualitatively similar results to Fig. 5, as described in S.5 of the Supplemental Material [35].

In conclusion, we have shown that passive microwave circulators can feasibly be built from a ring of superconducting tunnel junctions. The circuits can be integrated on chip with current fabrication technology and do not require any additional microwave or rf circuitry. The operating bandwidth is limited by the achievable waveguide coupling strength and can reach > 500 MHz for reasonable parameters. Due to the anharmonic spectrum of the central ring structure, nonlinearities are significant and the scattering matrix is strongly power dependent. The dual implementations we propose are reasonably insensitive to disorder and noise in bias charges. At their current state of development, the fabrication of QPS wires is less repeatable than JJ's; however, there may be applications for each implementation.

We thank A. Blais, T. Duty, S. Filip, W. Guichard, N. Roch, H. Rotzinger, P. Scarlino, and S. Skacel for discussions and comments. This work was supported by the Australian Research Council under the Discovery and Centre of Excellence funding schemes (Projects No. DP140100375, No. CE110001013, and No. CE170100039). Computational resources were provided by the NCI National Facility systems at the Australian National University through the National Computational Merit Allocation Scheme supported by the Australian government.

*c.muller2@uq.edu.au

- [1] C. L. Hogan, The ferromagnetic Faraday effect at microwave frequencies and its applications, *Bell Syst. Tech. J.* **31**, 1 (1952).
- [2] C. L. Hogan, The ferromagnetic Faraday effect at microwave frequencies and its applications, *Rev. Mod. Phys.* **25**, 253 (1953).
- [3] J. Clarke and F. K. Wilhelm, Superconducting quantum bits, *Nature (London)* **453**, 1031 (2008).
- [4] J. Q. You and F. Nori, Atomic physics and quantum optics using superconducting circuits, *Nature (London)* **474**, 589 (2011).
- [5] X. Gu, A. F. Kockum, A. Miranowicz, Y.-x. Liu, and F. Nori, Microwave photonics with superconducting quantum circuits, *Phys. Rep.* **718–719**, 1 (2017).
- [6] P. Lodahl, S. Mahmoodian, S. Stobbe, P. Schneeweiss, J. Volz, A. Rauschenbeutel, H. Pichler, and P. Zoller, Chiral quantum optics, *Nature (London)* **541**, 473 (2017).
- [7] S. R. Sathyamoorthy, L. Tornberg, A. F. Kockum, B. Q. Baragiola, J. Combes, C. M. Wilson, T. M. Stace, and G. Johansson, Quantum Nondemolition Detection of a Propagating Microwave Photon, *Phys. Rev. Lett.* **112**, 093601 (2014).
- [8] C. Müller, J. Combes, A. R. Hamann, A. Fedorov, and T. M. Stace, Nonreciprocal atomic scattering: A saturable, quantum Yagi-Uda antenna, *Phys. Rev. A* **96**, 053817 (2017).
- [9] B. Peng, Ş. K. Özdemir, F. Lei, F. Monifi, M. Gianfreda, G. L. Long, S. Fan, F. Nori, C. M. Bender, and L. Yang, Parity-time-symmetric whispering-gallery microcavities, *Nat. Phys.* **10**, 394 (2014).
- [10] J. Koch, A. A. Houck, K. L. Hur, and S. M. Girvin, Time-reversal-symmetry breaking in circuit-QED-based photon lattices, *Phys. Rev. A* **82**, 043811 (2010).
- [11] A. Kamal, J. Clarke, and M. H. Devoret, Noiseless non-reciprocity in a parametric active device, *Nat. Phys.* **7**, 311 (2011).
- [12] N. A. Estep, D. L. Sounas, J. Soric, and A. Alu, Magnetic-free non-reciprocity and isolation based on parametrically modulated coupled-resonator loops, *Nat. Phys.* **10**, 923 (2014).
- [13] K. M. Sliwa, M. Hatridge, A. Narla, S. Shankar, L. Frunzio, R. J. Schoelkopf, and M. H. Devoret, Reconfigurable Josephson Circulator/Directional Amplifier, *Phys. Rev. X* **5**, 041020 (2015).
- [14] F. Lecocq, L. Ranzani, G. A. Peterson, K. Cicak, R. W. Simmonds, J. D. Teufel, and J. Aumentado, Nonreciprocal Microwave Signal Processing with a Field-Programmable Josephson Amplifier, *Phys. Rev. Applied* **7**, 024028 (2017).
- [15] A. Kamal and A. Metelmann, Minimal Models for Nonreciprocal Amplification Using Biharmonic Drives, *Phys. Rev. Applied* **7**, 034031 (2017).
- [16] K. Fang, J. Luo, A. Metelmann, M. H. Matheny, F. Marquardt, A. A. Clerk, and O. Painter, Generalized non-reciprocity in an optomechanical circuit via synthetic magnetism and reservoir engineering, *Nat. Phys.* **13**, 465 (2017).
- [17] A. Metelmann and A. A. Clerk, Nonreciprocal Photon Transmission and Amplification via Reservoir Engineering, *Phys. Rev. X* **5**, 021025 (2015).
- [18] J. Kerckhoff, K. Lalumière, B. J. Chapman, A. Blais, and K. W. Lehnert, On-Chip Superconducting Microwave

- Circulator from Synthetic Rotation, *Phys. Rev. Applied* **4**, 034002 (2015).
- [19] B. J. Chapman, E. I. Rosenthal, J. Kerckhoff, B. A. Moores, L. R. Vale, G. C. Hilton, K. Lalumière, A. Blais, and K. W. Lehnert, Widely Tunable On-Chip Microwave Circulator for Superconducting Quantum Circuits, *Phys. Rev. X* **7**, 041043 (2017).
- [20] E. I. Rosenthal, B. J. Chapman, A. P. Higginbotham, J. Kerckhoff, and K. W. Lehnert, Breaking Lorentz Reciprocity with Frequency Conversion and Delay, *Phys. Rev. Lett.* **119**, 147703 (2017).
- [21] T. M. Stace, C. H. W. Barnes, and G. J. Milburn, Mesoscopic One-Way Channels for Quantum State Transfer via the Quantum Hall Effect, *Phys. Rev. Lett.* **93**, 126804 (2004).
- [22] G. Viola and D. P. DiVincenzo, Hall Effect Gytrators and Circulators, *Phys. Rev. X* **4**, 021019 (2014).
- [23] A. C. Mahoney, J. I. Colless, S. J. Pauka, J. M. Hornibrook, J. D. Watson, G. C. Gardner, M. J. Manfra, A. C. Doherty, and D. J. Reilly, On-Chip Microwave Quantum Hall Circulator, *Phys. Rev. X* **7**, 011007 (2017).
- [24] A. C. Mahoney, J. I. Colless, L. Peeters, S. J. Pauka, E. J. Fox, X. Kou, L. Pan, K. L. Wang, D. Goldhaber-Gordon, and D. J. Reilly, Zero-field edge magnetoplasmons in a magnetic topological insulator, *Nat. Commun.* **8**, 1836 (2017).
- [25] R. Barends *et al.*, Digitized adiabatic quantum computing with a superconducting circuit, *Nature (London)* **534**, 222 (2016).
- [26] N. K. Langford, R. Sagastizabal, M. Kounalakis, C. Dickel, A. Bruno, F. Luthi, D. J. Thoen, A. Endo, and L. DiCarlo, Experimentally simulating the dynamics of quantum light and matter at ultrastrong coupling, *Nat. Commun.* **8**, 1715 (2017).
- [27] J. Braumüller, M. Marthaler, A. Schneider, A. Stehli, H. Rotzinger, M. Weides, and A. V. Ustinov, Analog quantum simulation of the Rabi model in the ultra-strong coupling regime, *Nat. Commun.* **8**, 779 (2017).
- [28] J. E. Mooij and Yu. V. Nazarov, Superconducting nanowires as quantum phase-slip junctions, *Nat. Phys.* **2**, 169 (2006).
- [29] O. V. Astafiev, L. B. Ioffe, S. Kafanov, A. Yu. Pashkin, K. Yu. Arutyunov, D. Shahar, O. Cohen, and J. S. Tsai, Coherent quantum phase slip, *Nature (London)* **484**, 355 (2012).
- [30] J. T. Peltonen, O. V. Astafiev, Yu. P. Korneeva, B. M. Voronov, A. A. Korneev, I. M. Charaev, A. V. Semenov, G. N. Golt'sman, L. B. Ioffe, T. M. Klapwijk, and J.-S. Tsai, Coherent flux tunneling through NbN nanowires, *Phys. Rev. B* **88**, 220506 (2013).
- [31] J. T. Peltonen, Z. H. Peng, Yu. P. Korneeva, B. M. Voronov, A. A. Korneev, A. V. Semenov, G. N. Golt'sman, J.-S. Tsai, and O. V. Astafiev, Coherent dynamics and decoherence in a superconducting weak link, *Phys. Rev. B* **94**, 180508 (2016).
- [32] J. R. Friedman and D. V. Averin, Aharonov-Casher-Effect: Suppression of Macroscopic Tunneling of Magnetic Flux, *Phys. Rev. Lett.* **88**, 050403 (2002).
- [33] C. Müller, J. Bourassa, and A. Blais, Detection and manipulation of Majorana fermions in circuit QED, *Phys. Rev. B* **88**, 235401 (2013).
- [34] U. Vool and M. Devoret, Introduction to quantum electromagnetic circuits, *Int. J. Circuit Theory Appl.* **45**, 897 (2017).
- [35] See Supplemental Material at <http://link.aps.org/supplemental/10.1103/PhysRevLett.120.213602>, for details of the derivation, parameters used in the simulation and additional supporting results.
- [36] J. Combes, J. Kerckhoff, and M. Sarovar, The SLH framework for modeling quantum input-output networks, *Adv. Phys.* **X 2**, 784 (2017).
- [37] B. Q. Baragiola, R. L. Cook, A. M. Brańczyk, and J. Combes, N -photon wave packets interacting with an arbitrary quantum system, *Phys. Rev. A* **86**, 013811 (2012).
- [38] B. Fan, G. Johansson, J. Combes, G. J. Milburn, and T. M. Stace, Nonabsorbing high-efficiency counter for itinerant microwave photons, *Phys. Rev. B* **90**, 035132 (2014).
- [39] B. Q. Baragiola and J. Combes, Quantum trajectories for propagating Fock states, *Phys. Rev. A* **96**, 023819 (2017).
- [40] P. Forn-Díaz, J. J. García-Ripoll, B. Peropadre, J.-L. Orgiazzi, M. A. Yurtalan, R. Belyansky, C. M. Wilson, and A. Lupascu, Ultrastrong coupling of a single artificial atom to an electromagnetic continuum in the nonperturbative regime, *Nat. Phys.* **13**, 39 (2017).
- [41] F. Yoshihara, T. Fuse, S. Ashhab, K. Kakuyanagi, S. Saito, and K. Semba, Superconducting qubit-oscillator circuit beyond the ultrastrong-coupling regime, *Nat. Phys.* **13**, 44 (2017).
- [42] D. Vion, A. Aassime, A. Cottet, P. Joyez, H. Pothier, C. Urbina, D. Esteve, and M. H. Devoret, Manipulating the quantum state of an electrical circuit, *Science* **296**, 886 (2002).
- [43] J. Koch, T. M. Yu, J. M. Gambetta, A. A. Houck, D. I. Schuster, J. Majer, A. Blais, M. H. Devoret, S. M. Girvin, and R. J. Schoelkopf, Charge insensitive qubit design derived from the Cooper pair box, *Phys. Rev. A* **76**, 042319 (2007).
- [44] J. M. Fink, R. Bianchetti, M. Baur, M. Göppl, L. Steffen, S. Filipp, P. J. Leek, A. Blais, and A. Wallraff, Dressed Collective Qubit States and the Tavis-Cummings Model in Circuit QED, *Phys. Rev. Lett.* **103**, 083601 (2009).
- [45] W. D. Oliver (private communication).
- [46] S. Skacel and H. Rotzinger (private communication).